JACC Vol. 8, No. 3
September 1986:682–92

Quantitation of Regional Myocardial Function by Cine Computed Tomography: Pharmacologic Changes in Wall Thickness

PETER LANZER, MD, JEFFREY GARRETT, MD, MARTIN J. LIPTON, MD, FACC, ROBERT GOULD, PHD, RICHARD SIEVERS, BS, WILLIAM O'CONNELL, BS, ELIAS BOTVINICK, MD, FACC, CHARLES B. HIGGINS, MD, FACC

San Francisco, California

To determine the capability of high speed computed transmission tomography to quantitate regional wall thickening dynamics over a wide range of physiologic states, left ventricular wall thickening was studied in nine anesthetized mongrel dogs in the control state and during separate infusions of dobutamine (10 μg/kg per min) and phenylephrine (25 μg/kg per min). After an intravenous bolus of contrast medium the heart was imaged from base to apex with serial transverse images in eight short-axis cine computed tomographic planes. In each dog during each experimental condition, 50 ms scans spanning the cardiac cycle were acquired at each anatomic level. Left ventricular epicardial and endocardial boundaries were identified on end-diastolic and end-systolic images at the equatorial left ventricular planes by an objective threshold contour method validated in a series of experiments performed on ex vivo anatomic specimens. End-diastolic and end-systolic frames were automatically realigned by superposition of epicardial centers of gravity and then rotated using a cross correlation function. The left ventricular wall thickness was measured manually at 16 points around the circumference by two independent observers.

For the group of dogs the average percent wall thickening was 40.5 ± 28.2% and varied among segments from 18 to 70% in the control state. After dobutamine was administered, significant increases in heart rate and cardiac output ($p \leq 0.01$) were accompanied by an increase in the average wall thickening (73.6 ± 51.2%; $p \leq 0.001$) in the left ventricle; the average wall thickening among segments ranged from 46 to 97%. After phenylephrine administration, significant increases in mean blood pressure and cardiac output ($p \leq 0.01$) were noted along with a significant increase in average left ventricular wall thickening (60.3 ± 52.5%; $p \leq 0.001$). Despite an overall increase in the percent wall thickening, no statistically significant changes in segmental contraction pattern between control and drug intervention states were observed. The wall thickness measurements were highly reproducible between the two independent readers (reliability coefficient = 0.99).

Cine computed tomography-derived measurements can potentially be used for quantitative assessment of left ventricular wall thickening dynamics of a single heartbeat during acute interventions, such as the administration of drugs.

(J Am Coll Cardiol 1986;8:682–92)

Quantitative assessment of wall thickening dynamics is an important marker of left regional ventricular function. Increase in wall thickness in chronic pressure and volume overload of the left ventricle is a major compensatory factor in normalizing ventricular wall stress in these states (1–3). Changes in segmental ventricular wall thickness and thickening have been identified during the early stages of acute myocardial ischemia (4–6).

Precise and continuous measurements of regional wall thickness have been attained in experimental animals using ultrasonic crystals implanted across the myocardial wall and with other experimental techniques (7–13). In patients, left ventricular wall thickness has been assessed by contrast ventriculography (14–21) and M-mode and two-dimen-

From The Departments of Radiology and Medicine (Cardiology Division), Cardiovascular Research Institute, University of California, San Francisco, California. Dr. Lanzer is supported in part by Deutsche Forschungsgemeinschaft, Bonn, West Germany and the Ciba Foundation, Summit, New Jersey. Dr. Garrett is a recipient of Individual Research Fellowship HL-06944 from the National Institutes of Health, Bethesda, Maryland. Dr. Botvinick is an established investigator of the American Heart Association and is supported in part by a grant from the George D. Smith Fund, San Francisco, California. This work is also supported in part by National Institutes of Health Grant 1 R0133424, the Research and Education Foundation of the Department of Radiology, University of California, San Francisco and Imatron, Inc., South San Francisco, California.

Manuscript received August 20, 1985; revised manuscript received April 8, 1986, accepted April 16, 1986.

Address for reprints: Peter Lanzer, MD, Department of Cardiology, Moffitt Hospital, M-1186, University of California School of Medicine, San Francisco, California 94143.

0735-1097/86/$3.50

sional echocardiography (22–27). However, there are some limitations to the precision of these clinical techniques. With angiography, planar projection of a three-dimensional geometric image reduces the accuracy of measurements and each measurement can only be made for the small segment of the left ventricular wall that can be placed perpendicular to the X-ray beam and can be rotated away from overlapping cardiac structures. Consequently, important segments of ventricular wall are excluded from evaluation. Major disadvantages of echocardiographic measurements are equivocal and variable edge detection around the circumference of the left ventricular chamber, especially in technically difficult studies.

Recently, computed tomography has been proposed for measurements of regional left ventricular dimensions and dynamics. Computed X-ray tomography increases the reproducibility and geometric relevance of wall thickness measurements (28–30). However, poor temporal resolution with standard computed tomographic scanners has prevented wide clinical acceptance of this technique for the evaluation of cardiac function. The cine computed tomographic scanner has overcome this limitation by acquiring scans at multiple levels with an exposure time of 50 ms. The scanner has several capabilities useful for monitoring wall thickening dynamics, such as distinct spatial separation of left ventricular segments, sharp and uniform edge definition and adequate temporal resolution.

The purpose of this study was to: 1) develop objective methods for quantitating regional wall thickening dynamics by cine computed tomography; 2) determine the pattern and variability of wall thickening around the circumference of the left ventricle; and 3) assess the capability of cine computed tomography for quantitating the effect of acute interventions on regional wall thickening dynamics. To induce changes in wall thickening, dobutamine, a positive inotropic agent, and phenylephrine, a potent vasoconstrictor with a dose-dependent positive inotropic effect, were utilized. The objectives were not to specifically describe the hemodynamic effects of the two drugs; they were merely employed to induce acute steady state changes in wall thickening dynamics.

Methods

Experimental protocol. Nine mongrel dogs weighing 20 to 32 kg were anesthetized (25 mg/kg sodium pentobarbital intravenously and 10 mg/kg Innovar-vet intravenously) and intubated. Respiration was maintained at 16 breaths/min with a Harvard pump respirator. For cardiac output measurements, a 7F Swan-Ganz thermodilution catheter was positioned in the pulmonary artery through the femoral vein. For blood pressure measurements, a 12 gauge catheter was inserted into the femoral artery and connected to a Statham P23Db transducer. A separate catheter was introduced into the superior vena cava through the internal jugular vein for contrast medium administration. For heart rate monitoring and triggering of imaging sequences, three electrodes were attached to the dog's limbs.

Each dog was placed in the scanner in the right decubitus position. The long axis of the heart was defined in the first four dogs by two-dimensional echocardiography. To image the heart in short-axis views, the table of the scanner was typically slewed 20° to the left and tilted caudally 7°. In the remaining five studies, the dogs were positioned in this standardized position for short-axis views.

Measurements. Measurements were performed in the control state and sequentially after a steady state response was reached during the intravenous infusion of dobutamine (10 μg/kg per min) and phenylephrine (25 μg/kg per min). For each drug this was typically 20 minutes after initiation of the infusion. To accomplish simultaneous opacification of both ventricles, imaging runs were initiated 10 seconds after the beginning of the 4 second injection of a 30 cc bolus of 50% diluted iothalamate sodium (Conray 400). In this study, the bolus of the contrast medium was injected into the superior vena cava. However, when timing of bolus injection is adjusted to circulation time, peripheral venous injection can be used with equal results. During imaging, ventilation was suspended at a low inspiratory level. An electrocardiogram and arterial blood pressure were continuously recorded. Simultaneously, at least two measurements of thermodilution cardiac output were obtained in the control state and at steady state during each intervention. In each dog the average cardiac output, heart rate and mean blood pressure in each state were assessed.

Tomographic imaging. Typically, eight short-axis views were required to encompass the entire heart. Thus, two imaging runs, each spanning four anatomic levels usually during two consecutive heart beats, were acquired. From the eight anatomic levels in each dog, the equatorial left ventricular plane was selected for image analysis. Equatorial planes were selected to minimize errors introduced by incongruencies between cardiac anatomy and transaxial imaging methods, such as apex to base shortening, partial volume effects and oblique ventricular wall transsection by the imaging planes in the distal portion of the left ventricle. The left ventricular equatorial plane was defined as the plane of the eight scans encompassing the heart on which planimetry measured the largest area circumscribed by the endocardium at end-diastole in each state for each dog. At these identical tomographic planes, end-diastolic and end-systolic frames were identified as images corresponding closest to the upslope of the electrocardiographic R wave and last quarter of the T wave, respectively. End-diastolic, end-systolic and intermediate points within a cardiac cycle were defined as intervals of the 50 ms exposure length, plus 8 ms interexposure intervals.

JACC Vol. 8, No. 3
September 1986:682–92

Imaging sequence. The Imatron C-100 cine computed tomographic scanner was utilized in this study (31). The fast scan time is achieved by eliminating all mechanical motion, which in conventional computed tomographic scanners causes scan times of several seconds. The cine computed tomographic scanner produces an electron beam that is focused and deflected by time variable magnetic fields onto curved tungsten target rings that partially surround the patient. The X-ray beam is formed at the point where the electron beam strikes a target and is moved around the patient by deflecting the electron beam along a target ring. Because the scanner has two detector rings, two 8 mm thick adjacent slices with a 2 mm interslice gap are acquired simultaneously in the 50 ms scan time. Each 50 ms scan is followed by an 8 ms interscan delay so that, at a given level, the scanning rate is 16 scans/s. With the plane of an image, a resolution less than 2 mm is achieved.

In this study, imaging sequences were initiated by the electrocardiogram either at the R wave or after a preset delay from the R wave and generally consisted of 14 scans that were required to span the entire cardiac cycle. The resulting images were reconstructed from a matrix of 256 × 256 picture elements and displayed on a black and white monitor with the brightness of each volume element linearly proportional to the X-ray attenuation coefficient of the tissues examined (32). These attenuation coefficients were recorded as Hounsfield computed tomographic numbers according to the established relations with respect to the apparent density of water (33).

Image Analysis

Edge definition. Left ventricular endocardial and epicardial and right ventricular septal boundaries were identified using computer-assisted parallel search method with thresholding. This technique has been selected as an adequate and relatively simple approach for boundary definition for cine computed tomography-derived images where there is complete mixing of contrast medium and homogeneous opacification of the cardiac chambers. The process of cardiac border definition utilized in this study consisted of the following steps: 1) definition of edge operators, that is, Hounsfield computed tomographic numbers representing the left ventricular edge value in the individual image (see Appendix A); 2) highlighting pixels with calculated edge values using a bright flashing or video overlay, referred to as a blink mode; and 3) manually tracing the left ventricular border on enlarged and displayed images using a trackball.

To avoid inaccuracies in edge definitions in in vivo images with an uneven distribution of contrast medium within the left ventricular cavity, up to four edge pixel values were calculated for the variably opacified regions of the left ventricle. After evaluation of the edge operators for each image, boundaries were manually traced on the video screen by connecting pixels with edge values highlighted in the blink mode. As edge pixels were displayed close to each other errors due to filling in gaps were minimized. Figure 1 demonstrates boundary definition in end-diastolic and end-systolic frames.

Analysis of regional left ventricular wall thickening. To account for the translational and rotational movement of the heart within the thorax during the cardiac cycle we realigned end-diastolic and end-systolic frames as follows: 1) manually traced epicardial end-diastolic and end-systolic left ventricular edges were automatically digitized and the corresponding coordinates of the centroids were calculated. Then, end-diastolic and end-systolic centroids were superimposed; 2) the computer generated a line parallel to the x axis of the image matrix through the superimposed centroids; 3) employing a cross correlation technique (34), end-diastolic and end-systolic left ventricular edges were compared and the longitudinal rotational angle was calculated (see Appendix B). Then end-systolic images were rotated corresponding to the calculated angle (Fig. 2). Epicardial edges were used for centroid definition and rotational realignment to reduce the effect of inhomogeneities in the regional wall thickening and radial segment shortening (35). In one animal (dog 5) the outer left ventricular edges were nearly circular and prevented an accurate assessment of the rotational angle. Images in this dog were manually rotated by superposition of the left ventricular papillary muscles. From realigned images end-systolic (WT_S) and end-diastolic (WT_D) wall thicknesses were manually measured at 16 points (22.5° intervals) as the smallest distance between the intersection of the radius with the endocardial/epicardial interfaces. Segments containing papillary muscles were not analyzed. Figure 3 shows the anatomic location of 16 wall thickness measurements.

Percent wall thickening (%WT) was computed by the formula:

$$\% \text{ WT} = \frac{(WT_S - WT_D) \times 100}{WT_D}$$

Cine computed tomography-derived wall thickness measurements were calculated in each state as a mean and standard deviation of: 1) all segments for each dog, 2) all dogs for each segment, and 3) all dogs and all segments. Interobserver variability was tested by obtaining wall thickness measurements by two independent readers.

Statistical analysis. Data were evaluated by analysis of variance with repeated measures using dummy variables in a multiple regression model as specified in Appendix C to determine 1) the significance of changes in hemodynamic variables and wall dimensions between control state and interventions, and 2) the significance of changes in the pattern of wall thickening among the experimental states. The pattern of wall thickening was defined by comparison of segments 2 through 16 with segment 1. Interobserver var-

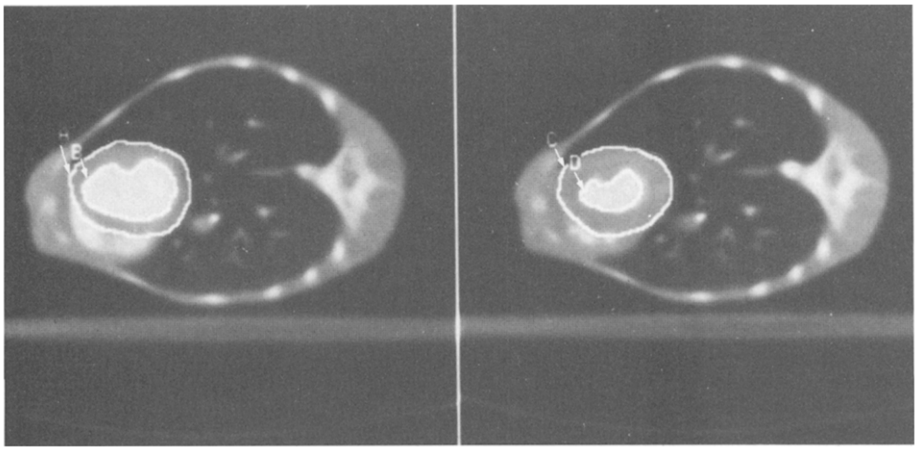

Figure 1. Definition of left ventricular edges. Shown are end-diastolic (**left**) and end-systolic (**right**) images at midventricular level. Left ventricular end-diastolic outer (A) and inner (B) boundaries and end-systolic outer (C) and inner (D) boundaries are displayed (**arrows**). Computed tomographic pixel values of ventricular edges are calculated and outlined as described in the Methods section.

iability was evaluated by analysis of variance with repeated measures.

Results

A total of 864 measurements of left ventricular wall thickness were taken. Because of the presence of the papillary muscles, 90 measurements were subsequently excluded from analysis. No statistically significant differences in wall thickness measurements between the two independent readers were observed (reliability coefficient = 0.99).

Comparison between control state and pharmacologic interventions. Table 1 provides a summary of the hemodynamic and computed tomographic data along with the statistical significance of any changes. Wall thickness and percent wall thickening represent means of all analyzed segments ± SD for individual dogs.

Dobutamine compared with a control state produced a significant increase in heart rate ($p \leq 0.002$), cardiac output, end-systolic wall thickness and percent wall thickening (all $p \leq 0.001$). Increases in mean blood pressure and end-diastolic wall thickness were not significantly different from the control state. Phenylephrine, compared with the control state, caused a significant increase in mean blood pressure, percent wall thickening (both $p \leq 0.001$) and cardiac output ($p \leq 0.05$).

Comparison between dobutamine and phenylephrine showed significantly higher heart rate ($p \leq 0.008$), end-diastolic ($p \leq 0.02$) and end-systolic ($p \leq 0.003$) wall thickness and percent wall thickening ($p \leq 0.001$) during dobutamine infusion. In contrast, mean blood pressure was significantly higher with phenylephrine ($p \leq 0.001$) and there was no significant difference in cardiac output.

Pattern of circumferential segmental wall thickening. Figure 4 shows the average percent wall thickening for all 16 segments in each state. In the control state, the average percent wall thickening among the segments varied between

Figure 2. Rotational realignment of end-diastolic and end-systolic frames. Shown are epicardial end-diastolic (**small dots**) and end-systolic (**large dots**) left ventricular contours in control state (**A**) and during dobutamine (**B**) and phenylephrine (**C**) infusions. The angle of end-diastolic to end-systolic rotation was calculated by cross correlation function.

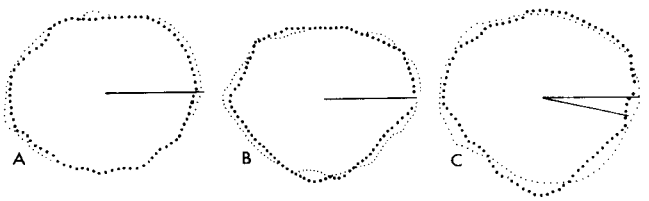

Figure 3. Anatomic definition of wall thickness measurements around the left ventricular circumference. Shown is a diagram of anatomic positions of 16 equally radially separated points (22.5°) where wall thickness measurements were taken. Points 1 to 3 and 16 correspond anatomically to the posterior wall, points 7 to 9 to the interventricular septum and points 10 to 15 to the anterolateral free wall of the left ventricle.

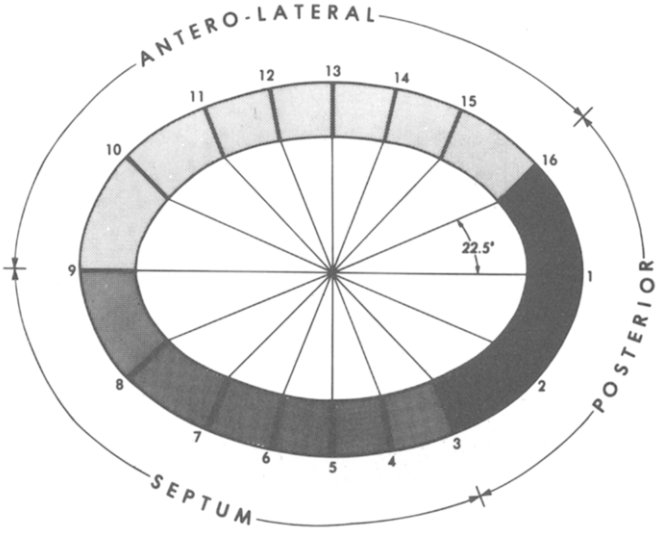

Table 1. Summary of Hemodynamic and Cine Computed Tomographic Image-Derived Measurements in Nine Dogs

Dog No.	HR (min^{-1})	BP (mm Hg)	CO (liters·min^{-1})	WT_D (mm)	WT_S (mm)	%WT	Rot (°)
			A. Control				
1	71	79.7	2.6	7.6 ± 1.5	11.9 ± 1.1	60.7 ± 28.4	+4
2	57	74.3	1.9	9.6 ± 1.6	15.8 ± 2.1	67.3 ± 26.0	+4
3	150	49.7	2.0	11.5 ± 1.6	13.6 ± 2.0	19.0 ± 18.9	+8
4	93	87.7	2.7	11.3 ± 1.4	13.9 ± 1.9	24.7 ± 16.0	+4
5	67	72.0	3.9	11.4 ± 2.0	14.5 ± 1.7	28.4 ± 16.5	+44
6	105	81.0	3.8	5.7 ± 1.0	7.6 ± 1.7	36.3 ± 35.4	0
7	65	73.3	2.1	7.9 ± 0.8	12.1 ± 1.5	54.2 ± 26.6	+4
8	80	106.0	3.2	9.8 ± 1.5	13.2 ± 1.8	36.4 ± 23.4	0
9	148	95.0	2.5	12.6 ± 3.0	15.7 ± 1.9	28.6 ± 22.3	0
Mean ± SD	93 ± 35	79.8 ± 15.9	2.7 ± 0.7	9.7 ± 2.7	13.2 ± 2.9	40.5 ± 28.8	
			B. Dobutamine				
1	60	93.3	3.3	8.1 ± 1.6	14.7 ± 1.5	86.4 ± 30.4	+4
2	85	91.7	4.0	9.4 ± 2.3	19.1 ± 2.2	112.6 ± 50.3	+4
3	140	73.7	3.1	11.3 ± 2.1	14.8 ± 2.1	32.0 ± 16.5	0
4	150	73.7	3.8	15.4 ± 3.1	20.7 ± 1.2	38.7 ± 26.6	+8
5	170	68.3	5.1	15.0 ± 2.7	22.6 ± 1.9	57.1 ± 39.2	+44
6	145	91.0	5.8	6.1 ± 1.4	9.6 ± 1.5	66.4 ± 53.9	+4
7	130	70.7	4.8	8.2 ± 1.3	20.7 ± 3.1	154.2 ± 43.5	+8
8	175	84.0	6.3	13.6 ± 1.4	19.0 ± 2.5	39.7 ± 14.7	0
9	145	110.0	4.7	10.6 ± 1.5	17.1 ± 1.7	63.5 ± 15.1	+4
Mean ± SD	133 ± 38	84.0 ± 13.7	4.5 ± 1.1	10.8 ± 3.6	17.6 ± 4.2	73.6 ± 51.2	
	$p \leq 0.02$*	NS*	$p \leq 0.001$*	NS*	$p \leq 0.01$*	$p \leq 0.001$*	
			C. Phenylephrine				
1	82	190.0	4.5	8.2 ± 1.2	9.4 ± 1.0	17.0 ± 17.7	−12
2	97	140.3	4.5	8.8 ± 1.1	17.3 ± 2.6	98.5 ± 35.8	−8
3	52	131.0	3.6	8.8 ± 1.9	13.5 ± 1.9	59.9 ± 29.4	+4
4	108	173.0	4.0	12.9 ± 2.4	18.3 ± 2.8	42.8 ± 13.9	+12
5	47	102.7	2.7	10.2 ± 1.7	15.6 ± 1.6	56.8 ± 28.5	−20
6	90	154.0	1.9	5.5 ± 1.5	7.5 ± 1.3	54.6 ± 42.0	0
7	67	150.6	3.4	7.9 ± 0.8	13.4 ± 2.7	73.6 ± 45.2	−12
8	105	116.0	7.5	9.6 ± 1.8	17.2 ± 2.2	82.7 ± 27.2	−12
9	83	125.3	2.9	10.5 ± 2.5	15.3 ± 2.3	51.9 ± 39.7	−8
Mean ± SD	81 ± 22.9	142 ± 27.6	3.9 ± 1.6	9.1 ± 2.5	14.1 ± 4.1	60.3 ± 42.5	
	NS†	$p \leq 0.001$†	$p \leq 0.05$†	NS†	NS†	$p \leq 0.001$†	
	$p < 0.001$‡	$p \leq 0.001$‡	NS‡	$p \leq 0.02$‡	$p \leq 0.01$‡	$p \leq 0.001$‡	

Diastolic and systolic wall thickness and percent wall thickening represent average values and standard deviations of all 16 segments in each dog. *p values are for comparison of dobutamine versus control; †p values are for comparison of phenylephrine versus control; ‡p values are for comparison of dobutamine versus phenylephrine. BP = mean blood pressure; CO = thermodilution cardiac output; HR = heart rate; Rot = rotation (− = clockwise longitudinal rotation, + = counterclockwise longitudinal rotation); WT_D = end-diastolic wall thickness; WT_S = end-systolic wall thickness; %WT = percent wall thickening.

17.6 and 70.0%; the mean percent wall thickening for each dog in the group ranged from 19.0 ± 18.9 to 67.3 ± 26.0% (Table 1A). Comparisons of segments 2 through 16 with segment 1 revealed significantly higher percent wall thickening in segments 4, 8, 9 and 11. A marginally significant higher percent wall thickening was observed in segments 5 and 10 ($p = 0.05$ and $p = 0.10$, respectively) (Table 2). In segment 12, because of the nearly invariable presence of the anterolateral papillary muscle, only two measurements were obtained. The low number of observations diminished the power of the statistical test and prevented significance despite the highest measured percent wall thickening.

Both dobutamine and phenylephrine produced a statistically significant upward shift in regional function as reflected by the pattern of wall thickening. With dobutamine, the average percent wall thickening among the segments ranged from 45.9 to 97.3% with an average increase among the segments of 33.6% above the control state (Table 2). With dobutamine, the mean percent wall thickening for each dog in the group ranged from 32.0 ± 16.5 to 159.2 ± 43.5% (Table 1B). Similarly, with phenylephrine, the average percent wall thickening among segments ranged from 23.9 to 91.7%, with an average increase among the segments of 20% above the control state (Table 2). The mean

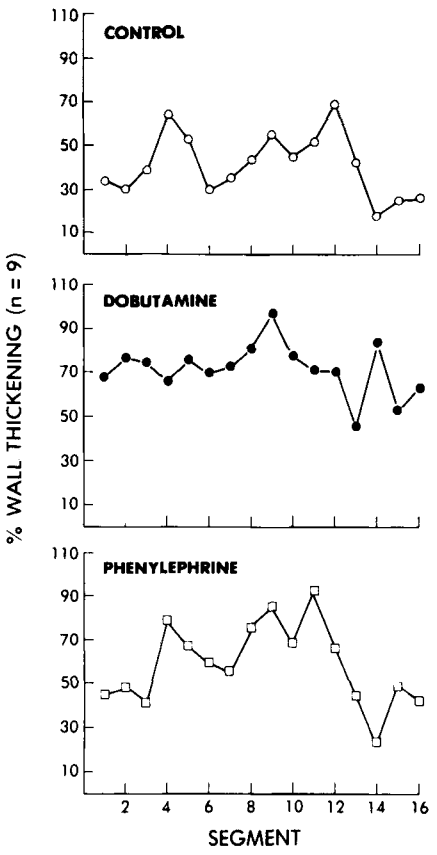

Figure 4. Average segmental percent wall thickening in studied states. Shown are diagrams of an average percent wall thickening as a function of segment position in all nine dogs. Repeated measures analysis of variance with multiple linear regression suggested that the basic pattern of percent wall thickening observed in the control state has not been significantly altered with pharmacologic interventions.

percent wall thickening for each dog in the group ranged from 17.0 ± 17.7 to 98.5 ± 35.8% (Table 1C). Figures 5 and 6 show typical examples of equatorial wall thickening during a single heartbeat in a control state and during an infusion of dobutamine.

The basic pattern of wall thickening in all dogs as a function of segment position around the circumference was not changed with dobutamine and phenylephrine. That is, both drugs only shifted the basic pattern observed in the control state upward without a significant change in shape of the basic pattern. This conclusion is based on the fact that interaction variables between segment position and drug in the multiple regression equation were not significant.

Longitudinal rotation of the heart from end-diastole to end-systole varied in control state and with dobutamine from 0 to +8° (in counterclockwise direction) with an average of +3°. With phenylephrine, the longitudinal rotation ranged from +12 to −12° with a mean angle of - 4.5° (in clockwise direction).

Discussion

Cine computed tomography in the current study showed considerable variability in wall thickening around the circumference of the left ventricle in the equatorial plane. It also revealed acute changes in average wall thickening and thickening of multiple individual segments in response to pharmacologic interventions. A characteristic pattern of wall thickening around the circumference was identified and this did not change significantly with the interventions.

Previous methods for measuring wall thickness. Clinical measurements of wall thickness have been previously obtained by contrast ventriculography (14–21), echocardiography (22–27), computed X-ray tomography (28–30) and nuclear magnetic resonance imaging (36). In contrast ventriculography the wall thickness is measured over a short segment of the left ventricular free wall (15). More recently, segmental measurements in long-axis views have been proposed (20). Using this technique, systolic wall thickening in a control state ranged from 30 to 150% (16–21) and typically exceeded values predicted from calculations of left ventricular mass (18) or those measured directly by implanted radiopaque markers (17). The discrepancy in experimental data has been explained by the possible inclusion of infolding trabeculation and papillary muscles in end-systolic measurements and uncertainties in identification of endocardial interfaces (17).

Table 2. Repeated Measures Analysis of Variance With Multiple Linear Regression and Dummy Variables

X Variable	Coefficient	p Value
Dobutamine	33.60267	0.00
Phenylephrine	20.03842	0.00
Segment		
2	0.21158	0.98
3	0.78032	0.99
4	20.81804	0.04
5	17.69840	0.08
6	5.12593	0.61
7	6.64487	0.50
8	19.31253	0.05
9	31.81881	0.00
10	16.62496	0.10
11	26.49502	0.02
12*	13.73631	0.35
13	−7.61789	0.67
14	−2.54684	0.89
15	−2.94437	0.77
16	−3.58049	0.72

Shown are the results of statistical analysis of drug interventions on overall and segmental percent wall thickening as a function of anatomic position around the left ventricular circumference. The coefficient associated with each X variable is interpreted as the change in percent wall thickening to segment 1 of the control condition.

*In this segment only two measurements were obtained.

JACC Vol. 8, No. 3
September 1986:682–92

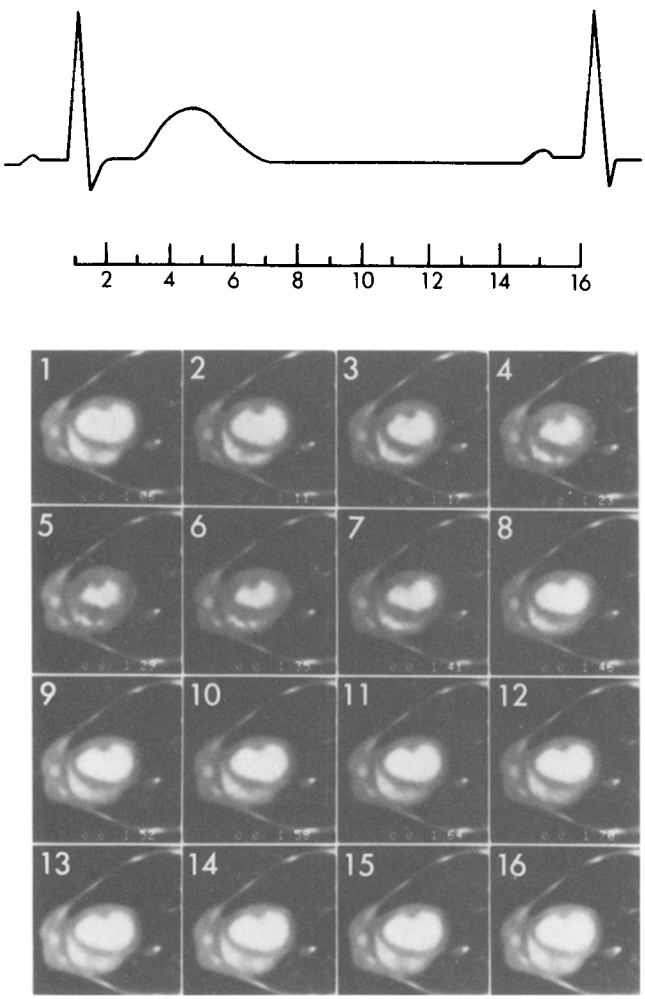

Figure 5. Cine computed tomographic image sequence acquired during a single heartbeat in the control state. Shown are 16 consecutive images of the dog heart at midventricular level with the corresponding electrocardiographic phase for each image. At a cardiac cycle length of 930 ms, corresponding to a heart rate of 65/min, 16 images were acquired in a single RR interval. Regional contraction is clearly demonstrated. At the given heart rate, image 6 approximates mechanical end-systole.

Two-dimensional and M-mode echocardiography have been proposed for the noninvasive assessment of wall thickening dynamics. In healthy subjects studied at different anatomic levels, Pandian et al. (25) measured a mean wall thickening of 71 ± 34% with a range of 0 to 150% in motion-corrected parasternal short-axis echocardiograms. The considerable variability in these data was attributed to biologic factors, such as regional differences in myocardial perfusion and myocardial fiber architecture and temporal asynchrony of contraction, and technical factors, such as difficulty in myocardial edge detection and intrathoracic cardiac motion. Significantly less variability has been reported by Haendchen et al. (26) from echocardiographic studies in dogs and humans. Measurements done at multiple left ventricular levels showed the mean systolic wall thickening increase from 20.5 ± 6.6 to 46.7 ± 11.5% and from 23.9 ± 5.6 to 28.9 ± 7.6% from base to apex in dogs and healthy humans, respectively. Furthermore, relatively higher systolic wall thickening in the posterolateral and anteroseptal segments were noted.

Imaging strategy: methodologic considerations. In the current study we report a new technique for quantitation of regional systolic wall thickening from a single heartbeat utilizing short-axis cine computed tomograms. This technique has some potential limitations, such as uncertainties regarding the selection of the centroid and efficacy of the cross correlation technique when applied to ventricles with regional contraction abnormalities. In addition, we report the results of serial wall thickness measurements by cine computed tomography in a wide range of pharmacologically altered contractile states. The current technique for quantitating wall thickening is highly reproducible and seems appropriate for characterizing the acute change in wall thickening dynamics induced by pharmacologic interventions. For this purpose a short-axis view was defined to minimize obliquity of the wall thickness measurement and variability in the degree of obliquity among segments. To define left ventricular myocardial edges, we employed a computer-assisted parallel search method with thresholding. This tech-

Figure 6. Cine computed tomographic image sequence acquired during a single heartbeat after dobutamine infusion. Eight consecutive 50 ms images are shown. At a cardiac cycle length of 470 ms, corresponding to a heart rate of 130/min, eight images were acquired in a single RR interval. Compared with the control state, overall increase in systolic wall thickness and a slight counterclockwise rotation of the heart can be appreciated. In this sequence, image 4 approximates mechanical end-systole.

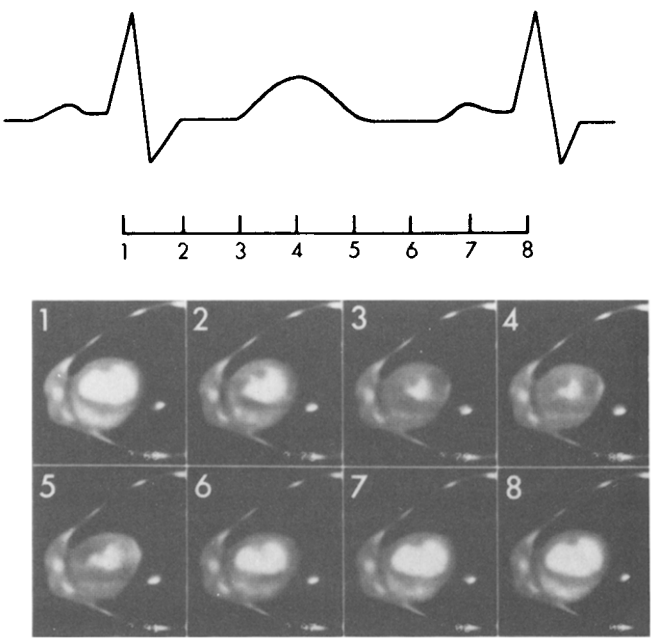

nique defines the edge but the actual border is traced by an operator. This does introduce some operator-dependent subjectivity. This edge detection procedure is relatively simple and proved accurate when wall thickness measurements were compared with the true wall thickness of ex vivo anatomic specimens. The threshold edge detection technique has not been verified with a technique such as sonomicrometry. Such an in vivo verification itself carries some uncertainties due to inherent imprecisions in placement and directionality of the endocardial sonomicrometric crystals. These uncertainties are avoided by the ex vivo calibrations employed in the current study.

Similarly, none of the more complex edge detection techniques based on estimating the radial gradient in signal intensity in individual pixels rather than a calculated threshold have been tested for comparison. Gradient techniques of edge detection can be, however, potentially useful in images with incomplete bolus mixing and inhomogeneous opacification of the left ventricular cavity. In these images, using the threshold technique, the determination of several threshold values was required.

To correct for translational and rotational cardiac motion in diastolic and systolic frames, we superimposed the end-diastolic and end-systolic centroids, defined as a center of mass of the epicardium, and assessed the phase angle of the end-diastolic and end-systolic epicardial edges calculated by cross correlation function.

No data are available to our knowledge on the choice of an optimal reference system, that is, internal floating versus external fixed, in cine computed tomography images. Similarly, data are lacking to compare the use of the endocardial versus epicardial centroids, or anatomic versus mathematic techniques for image realignment in internal frame of reference in cine computed tomographic studies. In this study, we used an epicardial edge rather than an endocardial edge to assess the centroid because of the unique edge definition (myocardium/lung tissue) and potentially a lesser effect of localized wall motion abnormalities on position of the centroid (35). The use of cross correlation function for rotational correction rather than reorientation by anatomic landmarks was favored as a potentially more objective observer-independent technique.

The realignment by cross correlation function appeared reliable, with the exception of images with nearly circular outer left ventricular edges. In these images cross correlation function cannot be applied and the use of anatomic landmarks is preferable. The hearts in the current study were normal and had similar epicardial shapes in systole and diastole. This method cannot be expected to be as reliable in the presence of ischemic heart disease with regional contraction abnormalities where shapes are different at end-diastole and end-systole. The rotational correction by cross correlation function was on average $+3°$ (counterclockwise) with a range of 0 to $+8°$ in a control state and with dobutamine, and was $-4.5°$ (clockwise) with a range of $+12$ to $-12°$ with phenylephrine. These results are similar to those obtained from radiopaque markers directly implanted into the canine endocardium (37) and from short-axis echocardiograms (38).

In this study images were taken during a 10 second period of suspended respiration and no corrections for respiratory movement of the heart were required. We analyzed only images at equatorial left ventricular planes, mainly for two reasons: 1) at this level the imaging plane should transsect the ventricular wall at right angles, that is, oblique transaxial images, or images with a significant partial volume effect should be avoided; and 2) the effect of apex to base shortening is minimized. The second consideration appears of little concern in normal contractile states, where changes in the length of the long axis are small (39) and will probably result in anatomic displacement that is smaller than the vertical thickness of a single imaging plane. However, with marked changes in chamber size and contractility the longitudinal displacement of the left ventricular segment relative to a fixed imaging plane will be more prominent and further data are needed to assess its significance. The wall motion occurring during the 50 ms exposure time will probably reduce the accuracy of the wall thickness measurements but should not affect their precision at comparable heart rates. For regional definition of wall thickening we measured end-diastolic and end-systolic wall thickness in the equatorial plane at 16 points around the circumference, each separated by 22.5°.

Wall thickening dynamics. Using the described technique, we measured regional wall thickening dynamics in a wide range of pharmacologically altered contractile states. In a control state the average systolic wall thickening among individual dogs varied from 19.0 to 67.3%, with an overall mean of 40.5%. During a continuous infusion of dobutamine the systolic wall thickening ranged from 32.0 to 159.2% among individual dogs, with an average of 73.6%. Similarly, infusion of phenylephrine increased wall thickening up to 17.0 to 98.5% among dogs with an average of 60.3%.

Analysis of the circumferential wall thickening pattern of the pooled data from all dogs in the control state revealed a significantly higher wall thickening in segment 4 (posteroseptal) and segments 8, 9 and 11 (anterolateral), when compared with segment 1. In segment 12 the highest mean percent wall thickening was measured in a control state. However, because only two measurements were obtained because of the frequent presence of papillary muscles, the reliability of the measured increase in wall thickening is diminished and the statistical test did not demonstrate a significant difference between segments 1 and 12.

With dobutamine and phenylephrine the overall wall thickening increased significantly by 33.6 and 20%, respectively, above the control state. However, despite increased wall thickening, the pattern of regional wall thick-

JACC Vol. 8, No. 3
September 1986:682–92

ening remained statistically unchanged with both drugs when compared with the control state.

Circumferential pattern of wall thickening: comparison with echocardiography. The systolic wall thickening measured in this study by cine computed tomography in the control state is similar to results obtained by two-dimensional echocardiography (25,26). The circumferential pattern of wall thickening defined by cine computed tomography suggests a higher systolic wall thickening, mainly in the anterolateral left ventricular free wall. In contrast, two-dimensional echocardiography revealed at a comparable anatomic level the highest wall thickening in the posterior and anterior left ventricular segments (26). The persistence of the circumferential pattern of wall thickening with pharmacologic interventions supports the relevance of cine computed tomography-derived measurements. The validity of these data is, however, somewhat limited by the size of the group of animals studied and the reduced number of observations in the anterolateral segments. Thus, in the absence of further data, observations on circumferential patterns of wall thickening remain empirical and further data are needed to confirm their pathophysiologic significance.

Conclusions. Cine computed tomography is a new technique for quantitative assessment of regional wall thickening dynamics in a defined tomographic plane. The method is noninvasive and can be objectively evaluated. Repeated assessment of regional ventricular function with this technique may permit quantitation of pharmacologic effects, potentially valuable to the clinical evaluation of patients with cardiovascular disease. However, the current technique should be applied with caution for ventricles with regional contraction abnormalities and more experimental data are needed in this regard.

Appendix A

Definition of edge operators by anatomic measurements. Because selection of the threshold value may be critical for the accuracy of the wall thickness measurements, definition of edge operators has been validated by anatomic measurements made from two excised hearts. The heart specimens were void of blood and orifices of the tricuspid and mitral valves were tightly sutured. Then two No. 7 Foley catheters were inserted across the semilunar valves into the right and left ventricular outflow tracts and tightly sutured. For imaging, the ventricles were filled with approximately 50 cc of 1:50 diluted Conray 400, positioned with the left ventricular long axis perpendicular to the imaging plane in the scanner, and eight 1 cm thick imaging transaxial planes indicated by laser beam were marked on the left ventricular anterior wall.

After imaging, the hearts were dissected along the imaging planes. The left ventricular borders of two midventricular planes in each heart were traced manually on the plastic overlay. Using the left ventricular anterior wall labels the tracings were realized with 1:1 enlarged cine computed tomographic images of these two levels and 16 angularly equidistant measurements of wall thickness around the circumference were taken. To calculate the edge operators we used empirically derived formulas, where endocardial edges were defined as pixels with a computed tomographic (CT) number defined as: $EN = M_{CT} + [(C_{CT} - M_{CT}) \cdot X]$, where M_{CT} = myocardial computed tomographic number, C_{CT} = intracavitary computed tomographic number and X = fixed percent threshold value. Epicardial edges were defined as pixels with a computed tomographic number $EP = L_{CT} + [(M_{CT} - L_{CT}) \cdot Y]$, where L_{CT} = lung parenchymal computed tomographic number, M_{CT} = myocardial computed tomographic number and Y = fixed percent threshold value. On the basis of our previous experience, values of X = 50, 70 and 80% and corresponding Y = 50, 30 and 20% were evaluated. Cine computed tomographic measurements employing values of X and Y of 50:50%, 70:30% and 80:20% combination of the threshold values were highly correlated with the true wall thickness measured from anatomic 1 cm thick slices taken along identical imaging planes. The respective correlation coefficients were $r = 0.88$ for X = 50%, Y = 50%; $r = 0.90$ for X = 70%, Y = 30%; and $r = 0.87$ for X = 80%, Y = 20%. However, among the threshold values, X = 70%, Y = 30% corresponded to the lowest 95% confidence interval and was selected for left ventricular edge detection. In this study no attempt has been made to validate the edge operator under in vivo conditions. Thus, assuming similar concentrations of contrast material within the ex vivo and in vivo ventricular cavities, the remaining effect of ventricular wall motion during 50 ms exposure time on edge definition remains to be determined.

Appendix B

Calculation of rotational angle. To account for longitudinal rotation of the heart between end-diastole and end-systole, the outer boundaries of the left ventricle in end-diastolic and end-systolic images were cross correlated (23). In our approach 90 contour radii were sampled with a radial distance of 4° around the circumference. Thus, offsetting the index of the radius by one was equivalent to a rotation of 4°. To select the rotation angle for the end-systolic contour, the integer offset k ranged from −11 to +11. For each value of k the cross correlation function CC_k was computed according to the formula:

$$CC_k = \sum_{j=1}^{90} R_j \cdot r_i,$$

where R_j = the length of the end-diastolic radius j; r_i = the length of the end-systolic radius i; and $i = \text{mod}\ (j + k - 1, 90) + 1$. The maximal value of cross correlation function (CC_k) selected the rotation angle = 4k.

Appendix C

Statistical analysis. Repeated measures analysis of variance with multiple linear regression and dummy variables was done to analyze the effect of drug interventions on 1) the hemodynamic variables; and 2) average values of wall thickness and percent wall

thickening and the pattern of percent wall thickening as a function of segmental position around the circumference.

The following formula describes the drug effect on hemodynamic and averaged tomographic variables:

$$Y = A_o + A_1 \text{ dobutamine} + A_2 \text{ phenylephrine} + \sum_{i=1}^{8} b_i \cdot \text{Dog}_i, \quad (1)$$

where dobutamine, phenylephrine and dog are dummy variables defined as:

$$\text{Dobutamine} = \begin{cases} 1 \text{ if dobutamine,} \\ 0 \text{ otherwise} \end{cases}$$

$$\text{Phenylephrine} = \begin{cases} 1 \text{ if phenylephrine,} \\ 0 \text{ otherwise} \end{cases}$$

$$\text{Dog} = \begin{cases} 1 \text{ if dog 1,} \\ -1 \text{ if dog 9,} \\ 0 \text{ otherwise.} \end{cases}$$

A_o is an estimate of the mean in the control state. A_1 and A_2 are estimates of the respective drug effects on the variable Y as compared with the control state. The last term of the equation,

$$\sum_{i=1}^{8} b_i \cdot \text{Dog}_i,$$

accounts for variability between dogs; that is, it takes into account the repeated measures experimental design.

The following formula describes the segmental changes in percent wall thickening (%WT):

$$\%WT = a_i \text{ dobutamine} + a_2 \text{ phenylephrine} + \sum_{i=1}^{8} b_i \text{ dog}_i \sum_{i=2}^{16} c_j \text{ segment}_j, \quad (2)$$

where dobutamine, phenylephrine and dog_i are dummy variables as described above and segment_j represents 15 dummy variables for the 16 segments with segment 1 as a reference and segment 2, segment 3 . . . segment 16 are defined as follows:

$$s_j = \begin{cases} 1 \text{ if segment j,} \\ 0 \text{ otherwise.} \end{cases}$$

The coefficient a_o is an estimate of the average percent thickening in segment 1 under control conditions. The coefficients a_1, a_2 and b_i in equation 2 are interpreted as described above for A_i, A_2 and B_i in equation 1. The additional coefficient c_j is interpreted as the average change of segment j from the average wall thickening observed in segment 1. For example, if segment 4 = 20.8, that is interpreted as percent wall thickening in segment 4 to be 20.8 percent units higher than segment 1.

We thank Bryan Slinker, PhD for excellent collaboration on statistical analysis of the data, Vojtech Licko, PhD for consultations and Shirley Semigran for typing and editing the manuscript.

References

1. Grossman W, Jones D, McLaurin LP. Wall stress and pattern of hypertrophy in the human left ventricle. J Clin Invest 1975;56:56–64.
2. Sasayama S, Ross J, Franklin D, Bloor CM, Bishop S, Dilly RB. Adaptation of the left ventricle to chronic pressure overload. Circ Res 1976;38:172–8.
3. Gaasch WH. Left ventricular radius to wall thickness ratio. Am J Cardiol 1979;43:1189–94.
4. Gallagher DP, Kamuda T, Koziol JA, McKown MD, Kemper WS, Ross J Jr. Significance of regional wall thickening abnormalities relative to transmural myocardial perfusion in anesthetized dogs. Circulation 1980;62:1266–74.
5. Pandian NG, Kerber RE. Two dimensional echocardiography in experimental coronary stenosis. II. Relationship between systolic wall thinning and regional myocardial perfusion in severe coronary stenosis. Circulation 1982;66:603–11.
6. Lieberman AN, Weiss JL, Jugdutt BL, et al. Two dimensional echocardiography and infarct size: relationship of regional wall motion and thickening to the extent of myocardial infarction in the dog. Circulation 1981;63:739–46.
7. Bugge-Asperhelm B, Leraand S, Kiil F. Local dimensional changes of the myocardium measured by ultrasonic technique. Scand J Clin Lab Invest 1969;29:361–71.
8. Guntheroth WG. Changes in left ventricular wall thickness during the cardiac cycle. J Appl Physiol 1974;36:308–12.
9. Sabbah HN, Marzilli M, Stein PD. The relative role of subendocardium and subepicardium in left ventricular mechanics. Am J Physiol 1981;270:H920–6.
10. Osakada G, Sasayama S, Kawai C, et al. The analysis of left ventricular wall thickness and shear by an ultrasonic triangulation technique in the dog. Circ Res 1980;47:173–81.
11. Gaasch WH, Bernard SA. The effect of acute changes in coronary blood flow on left ventricular end-diastolic wall thickness. Circulation 1977;56:593–7.
12. Sasayama S, Franklin D, Ross J Jr., Kemper WS, McKown D. Dynamic changes in left ventricular wall thickness and their use in analyzing cardiac function in the conscious dog. Am J Cardiol 1976;38:870–9.
13. Feigl O, Fry DL. Myocardial mural thickness during the cardiac cycle. Circ Res 1964;14:541–5.
14. Goldstein S, DeJong JW. Changes in left ventricular wall dimensions during regional myocardial ischemia. Am J Cardiol 1974;34:56–62.
15. Rackley CE, Dodge HT, Coble YD Jr, Hay RE. A method for determining left ventricular mass in man. Circulation 1964;29:666–71.
16. Hawthorne EW. Dynamic geometry of the left ventricle. Am J Cardiol 1966;18:566–73.
17. Mitchell JH, Wildenthal K, Mullins CB. Geometrical studies of the left ventricle utilizing biplane cinefluorography. Fed Proc 1969;28:1334–43.
18. Hugenholtz PG, Kaplan E, Hull E. Determination of left ventricular wall thickness by angiocardiography. Am Heart J 1969;78:513–22.
19. Eber LM, Greenberg HM, Cooke JM, Gorlin R. Dynamic changes in left ventricular free wall thickness in the human heart. Circulation 1969;39:455–64.
20. Bove AA. Radiographic evaluation of dynamic geometry of the left ventricle. J Appl Physiol 1971;31:227–34.
21. Gould KL, Kennedy JW, Frimer M, Pollack HG, Dodge HT. Analysis of wall dynamics and directional components of left ventricular contraction in man. Am J Cardiol 1976;38:322–31.
22. Troy BL, Pombo J, Rackley LE. Measurement of left ventricular wall thickness and mass by echocardiography. Circulation 1971;45:602–11.
23. Henry WL, Cardin JM, Ware JH. Echocardiographic measurements in normal subjects from infancy to old age. Circulation 1980;62:1054–61.
24. Reicheck N, Wilson J, Sutton MSJ, Plappart TA, Goldberg S, Hinschfeld JW. Noninvasive determination of left ventricular end-systolic stress: validation of the method and initial application. Circulation 1982;65:99–108.

25. Pandian NG, Skorton DJ, Coolins SM, Falscetti HL, Burke ER, Kerber RE. Heterogeneity of left ventricular segmental wall thickening and excursion in two dimensional echocardiograms of normal human subjects. Am J Cardiol 1983;51:1667–73.

26. Haendchen RV, Wyatt HL, Maurer G, et al. Quantitation of regional cardiac function by two-dimensional echocardiography. I. Patterns of contraction in the normal left ventricle. Circulation 1983;67:1234–45.

27. Feneley MP, Hickie JB. Validity of echocardiographic determination of left ventricular systolic wall thickening. Circulation 1984;70:226–32.

28. Miller SW, Dinsmore RE, Wittenberg J, Maturi RA, Powell WJ Jr. Right and left ventricular volumes and wall measurements: determination by computed tomography in arrested canine hearts. Am J Roentgenol 1977;129:257–61.

29. Skioldebrand LG, Ovenfors CO, Mavroudis C, Lipton MJ. Assessment of ventricular wall thickness in vivo by computed tomography. Circulation 1980;61:960–5.

30. Mattrey RF, Slutsky RA, Long SA, Higgins CB. In vivo assessment of left ventricular wall and chamber dynamics during transient myocardial ischemia using prospectively ECG-gated computerized transmission tomography. Circulation 1983;67:1245–51.

31. Boyd DP, Gould RG, Quinn JR, Sparks R, Stanley JH, Hermannsfeldt WB. A proposed dynamic cardiac 3D densitometer for early detection and evaluation of heart disease. IEEE Trans Nucl Sci 1979;NS-26:2724–7.

32. Jaschke W, Gould R, Assimakopoulos PA, Lipton MJ. Flow measurements with a high speed CT scanner. Radiology (submitted).

33. McCullough EC. Factors affecting the use of quantitation information from a CT scanner. Radiology 1977;124:99–107.

34. Sandor T, Paulin S, Hanlon WB. Left ventricular wall motion analysis using operator independent contour positioning. Comput Biomed Res 1984;17:129–42.

35. Nguyen T, Gould R. Personal communication.

36. Fisher M, van Schulthess G, Higgins CB. Multiphasic cardiac magnetic resonance imaging: normal regional left ventricular wall thickening. Am J Roentgenol 1985;145:27–30.

37. Walley RR, Grover M, Raff GL, Benge JW, Hanneford B, Glantz SA. Left ventricular dynamic geometry in the intact and open chest dog. Circ Res 1982;573–89.

38. Mirro MJ, Roger EW, Weyman AE, Feigenbaum H. Angular displacement of the papillary muscles during the cardiac cycle. Am J Cardiol 1979;38:327–33.

39. Rankin JS, McHale PA, Arentzen CE, Ling D, Greenfield JC Jr, Anderson RW. The three-dimensional dynamic geometry of the left ventricle in the conscious dog. Circ Res 1976;39:304–13.